24th INTERNATIONAL CONGRESS ON SOUND AND VIBRATION
23–27 July 2017, London

FINITE DIFFERENCE TIME DOMAIN MODELLING OF RADIATION FROM A POINT-EXCITED ELASTIC PLATE INTO A REVERBERANT SPACE

Nuno Ferreira, Carl Hopkins

Acoustics Research Unit, School of Architecture, University of Liverpool, Liverpool L69 7ZN,UK
emails: nunomgf@liverpool.ac.uk, carl.hopkins@liverpool.ac.uk

This paper concerns experimental validation of a Finite Difference Time Domain (FDTD) model for the vibroacoustic problem of a thin plate undergoing point excitation inside a small reverberation chamber. The dimensions of typical thin plates radiating into rooms make it computationally impractical to model the coupled problem without making some modifications in its geometry and physical properties of the model. These modifications were carried out in such a way as to preserve the same vibrational properties of the plate-room coupled model, while allowing for much larger time steps; hence reducing the total number of iterations necessary to complete the simulation. In the experiment validation, an aluminium plate was mechanically point excited inside a 13m^3 room using an electrodynamic shaker. The resulting sound pressure inside the room was measured using an array of microphones that were placed along a horizontal and vertical measurement grid covering its acoustic space. Results obtained using the FDTD model are compared with measurements in terms of contour plots using the transfer function of sound pressure to the applied force; these show close agreement.

Keywords: FDTD, plate, radiation, vibroacoustics

1. Introduction

This paper concerns Finite Difference Time Domain (FDTD) modelling of the interaction between the vibration field of a point-excited thin plate and the coupled reverberant sound field at low frequencies. Such a model can be problematic because the general FDTD formulation [1] using a uniform FDTD grid requires a large number of elements and small time steps. This is addressed in this paper using a new approach which brings significant computational advantages.

Approaches to model fine geometric details embedded in large FDTD models are primarily concerned with the use of non-uniform grids, parallelization of the FDTD computations and the use of dimension-reduced models. The parallelization of FDTD consists of splitting the routine calculations and memory over a number of CPU or GPU units, enabling faster computation times. In FDTD, parallelization has been implemented by a variety of authors in a number of research fields such as electrodynamics [2], vibration [3] and vibroacoustics [1]. The use of non-uniform grids (a technique also known as subgridding) allocates a finer grid resolution to regions that require more detail whilst using coarser grid elements elsewhere [2]. Sub-gridding has been applied to acoustics problems [4] but is seemingly not yet used in vibroacoustics. Dimension-reduced models use a 2D grid to represent structural elements rather than using solid elements. The procedure of converting a 3D solid structures into a 2D structure results in significant memory savings and reduced computation times. The 2D implementation of thin plates has been carried out using Kirchhoff-Love theory [5] and for 2D thick plates using Mindlin-Reissner theory [6].

In this paper, the first aspect that is considered is computational efficiency for which the problem of modelling a thin aluminium plate radiating into a reverberant room is reformulated. An advantage of this approach is its simplicity because it uses the standard FDTD model [1] and no extra code is needed. The second aspect concerns the experimental validation of the use of completely

general FDTD update equations which allow all kinds of wave motion, even though only bending wave modes are excited on the plate by using a perpendicular point force.

2. Theory

2.1 FDTD model

The FDTD approach implemented in this paper follows that described by Toyoda and Takahashi [1] where the authors describe the whole vibroacoustic field using two numerical variable fields: a velocity field (vector) and a stress field (tensor). However, in order to allow easier integration with previous work carried out in acoustic FDTD [7], the FDTD model in this paper considers three types of numerical fields: a pressure field (scalar), a velocity field (vector) and a stress field (tensor).The stress and velocity fields were used to model the structural medium, whereas the velocity and pressure fields were used to model wave propagation in the acoustic medium, including Perfectly Matched Layers (PMLs). The update equations used for the acoustic medium are discussed in detail by Kunz [8], and those for modelling the structural medium and corresponding boundary conditions are discussed in sections 2.1.1 and 2.1.4 respectively. The coupling between acoustic medium and solid structure is a sequential two-way coupling so that any change in the acoustic field propagates into the structural vibration field and vice-versa. In this work, the vibration field is excited with a source that causes it to radiate and give rise to a sound field in a room.

2.1.1 Structural wave propagation

A general formulation is used for the plate that allows simulation of all types of wave motion. The momentum equations used to simulate the structural material were formulated in terms of the relationship between the stress tensor acting on an element and the corresponding velocity of that element [1]. The basic constitutive model assumed for the structural medium is a linear isotropic viscoelastic Voigt-element [9]. Hence, the time domain physical tensor equations used to describe the propagation of vibration are [1]:

$$\rho \frac{\partial v_i}{\partial t} = \frac{\partial \sigma_{ji}}{\partial x_j} - \beta v_i \tag{1}$$

$$\frac{d\sigma_{ij}}{dt} = \lambda \varepsilon_{kk} \delta_{ij} + 2\mu \varepsilon_{ij} + \chi \frac{d\varepsilon_{kk}}{dt} \delta_{ij} + 2\gamma \frac{d\varepsilon_{ij}}{dt} \tag{2}$$

where ρ is the density, v_i is the velocity vector, σ_{ij} is the stress tensor, λ and μ denote the Lamé coefficients, β is a damping constant proportional to velocity, and χ and γ denote the viscosity damping constants. The variable ε_{ij} represents the rate-of-deformation tensor defined by:

$$\varepsilon_{ij} = \frac{1}{2}\left(\frac{\partial v_j}{\partial x_i} + \frac{\partial v_i}{\partial x_j} \right) \tag{3}$$

In order to implement the FDTD routine, Eqs. (1) and (2) were discretised to allow their explicit numerical solution. The variables were arranged in space according to a lattice described by Schroder *et al* [10] using a spatial resolution of Δx=0.13m, Δy=0.35m and Δz=0.39m.

2.1.2 Vibration source

The source used for the simulations was a vibration hard source. The normal stress component in the vertical direction (*z*-axis) of the vibration source element was assigned a time-dependence $\sigma_{zz}(t)$, which was followed irrespective of the state of its neighbour nodes. The driving function assigned to the source was the first time derivative of the Gaussian pulse as its spectrum contains no energy at 0Hz, which would represent static loading and deformation of the plate. This has the form:

$$\sigma_{zz}(t) = \sigma_o (t - t_o) e^{-\frac{(t-t_o)^2}{2\tau^2}} \tag{4}$$

2.1.3 Numerical receiver positions

Pressure receivers were positioned along uniform horizontal and vertical grids. The geometrical positioning of these grids matches that of the experimental grid used in the validation. The pressure impulse response collected at the receivers was Fourier transformed and divided by the spectrum of the driving function $F(\omega)$, in order to obtain a transfer function of pressure-to-force.

2.1.4 Boundary conditions

For the room, the acoustic boundary conditions are frequency-independent and are described in detail by Yokota *et al* [11]. For the plate, the implementation of simply supported boundary condition was carried out by assigning a value of zero to the vertical velocities that are located on the mid-plane of the boundaries of the plate. Since air was assumed to be an inviscid medium, the shear force adjacent to the surface of the plate was also set to zero. In terms of the velocity nodes occurring at the solid-air boundary, the implementation used here differs from that described by Yokota *et al* [12]. According to these authors, in a boundary between two media, the velocity update equation is split into two equations, involving a forward difference and a backward difference. These equations are then combined to form a new equation, where the space step across the boundary is divided by a factor of two and the density at the boundary between the two media is averaged.

In this paper the implementation of the solid-air boundary considers the update equations for the velocity elements that lie on the boundaries to be identical to regular velocity update equations and the density value considered is that attributed to the solid. This simplification requires that the spatial resolution along a given direction of the structure be defined by $\Delta x=L_z/(n\text{-}0.6)$ rather than $\Delta x=L_z/n$, where n is the number of normal stress nodes along a given direction. As an example, consider the spatial resolution along the thickness direction of the plate: it is necessary to assign at least two nodes of normal stress so that bending wave motion can propagate, where the top node is compressed and the bottom node is strained. In this case the space step required using our boundary conditions is 30% larger than that required using the approach described in Yokota *et al* [12]. This larger space step has computational benefits, since the time step can be larger.

2.1.5 Loss factors

No damping was considered for wave motion in air. For the plate, all dissipation of mechanical energy occurred due to the viscoelastic nature of the plate material as internal damping following the approach of Toyoda *et al* [13]. The damping constants β, γ and χ result in a frequency-dependent loss factor, similar to systems characterized by Rayleigh damping. The frequency-dependent loss factor of the plate was measured as described in section 3. The damping coefficients were calculated so that the resulting internal loss factor in FDTD would follow the loss factor of the actual plate as closely as possible. This gave the following damping coefficients: β =11,000 N.s.m^{-4} and γ=0 N.s.m^{-2} and χ=0 N.s.m^{-2}

2.2 Scaling of vibroacoustic fields

The Courant condition dictates the maximum possible value that can be used for the time step in the FDTD model [8]:

$$\Delta t \leq \frac{1}{c\sqrt{\left(\frac{1}{\Delta x}\right)^2+\left(\frac{1}{\Delta y}\right)^2+\left(\frac{1}{\Delta z}\right)^2}} \tag{5}$$

where c is the phase velocity of wave motion and Δx, Δy and Δz are the spatial resolutions in the x, y and z directions respectively. If a higher value for the time step is chosen to run the simulation, the corresponding solution will become unbound. The smaller the required time step, the longer it will take to run a simulation for a given time duration.

For vibroacoustic simulations, it is computationally expensive to simulate a large model whose spatial resolution is very fine where the structure-borne wave speeds are very high. In such cases,

this paper proposes an alternative formulation of the vibroacoustic problem which will yield much faster results when using standard FDTD [1]. The main problem when modelling a large vibroacoustic problem is that if the spatial resolution is kept constant, a large number of elements are required to represent the whole domain. In addition, since the spatial resolution is fine, the required time step will be very small as a consequence of the Courant condition (Eq. (5)). The proposed alternative is to model a larger structure that has the same vibration characteristics as the original structure and couple it to the acoustic medium because the use of a coarser spatial resolution will result in a larger time step. Once the equivalent structure is identified and processed, the results can then be scaled back to the original problem. Assuming the thickness direction of the plate to be coincident with the vertical z-axis, the following steps are used to scale the vibroacoustic model:
(1) A scaling factor s is chosen and a plate with the same eigenfrequencies as the original plate is identified where the sides of the scaled plate are $L_x' = sL_x$ and $L_y'=sL_y$ respectively. The thickness of the scaled plate is $h'=s^2h$.
(2) The new spatial resolution is $\Delta x'= s\Delta x$, $\Delta y'= s\Delta y$ and $\Delta z'= s^2\Delta z$. The dimensions of the acoustic space need to be scaled up by a factor of s to match the scaled dimensions of the plate and is modelled using the new resolutions $\Delta x'$, $\Delta y'$ and $\Delta z'$. This results in the use of less elements in the z-direction, since the space step is larger along this direction ($\Delta z'= s^2\Delta z > s\Delta z$). In order to keep the same acoustic eigenfrequencies, the speed of sound in air must be scaled using $c'=sc$.
(3) To keep the same characteristic acoustic impedance, the density of the air medium has to be scaled using $\rho'= \rho/s$.
(4) The magnitude of the driving-point mobility of the scaled plate is offset from the original plate by a factor of s^4. Therefore the results obtained should be scaled accordingly, in order to account for this offset in the magnitude of the driving-point mobilities.

This formulation has the advantage of using larger time steps and fewer elements. For the particular case of the aluminium plate coupled into a room in this paper, where s=6 is used, the total number of elements used to model the problem was 374,660 (including the PMLs) and the total number of time steps was 206,895. If no scaling was applied, the total number of elements would be 2,019,160 and the required number of time steps, for the same duration would be 6,694,777. Hence, the same code, without the scaling formulation, would be around 160 times slower.

An important limitation of the scaling formulation is that it cannot be applied to vibroacoustic problems with non-parallel plates (i.e. a cavity formed by six plates). In addition, as the thickness of the plate is increased, the frequency at which bending wave motion dominates is reduced [14]. If the original thin plate frequency limit is f_b, the limit for the corresponding scaled plate f_b' is given by $f_b'= f_b/s^2$ and the simulation results are not valid above this limit.

3. Experimental procedure

A 5mm thick aluminium plate (1.2m x 0.8m) was placed inside a small, empty reverberation chamber (1.83m x 2.87m x 2.48m). Sound pressure measurements were taken using two grids, one horizontal grid (15 x 11 positions) and one vertical grid (13 x 11) – see Fig. 1. The interval between consecutive positions in the y-direction was 0.18m for both horizontal and vertical grids. The space interval was 0.2m in the x and z-directions, for the horizontal and vertical grid respectively. The distance from the horizontal grid to the floor was 0.84m. The distance from the vertical plane to the back wall of the room was 0.82m. The uncertainty in the microphone positioning was +/-2cm.

The plate was positioned at a height of 0.78m above the floor, resting on a metal frame and simply supported around its edges using an aluminium frame described by Yin and Hopkins [15] – see Fig. 2. To provide damping similar to the Rayleigh curve, a viscoelastic damping material (Sylomer) was fixed onto the surface of the plate using a number of different configurations. The loss factors were then measured using the 3dB down-point method form the magnitude of the driv-

ing-point mobility. Among the several configurations tested, the diamond shape configuration shown in Fig. 2a was used as the damping approximately followed a Rayleigh damping curve.

The source was excited using an electrodynamic shaker connected to the plate via a force transducer. The force transducer was fixed onto the bottom side of the plate as shown in Fig. 2b.

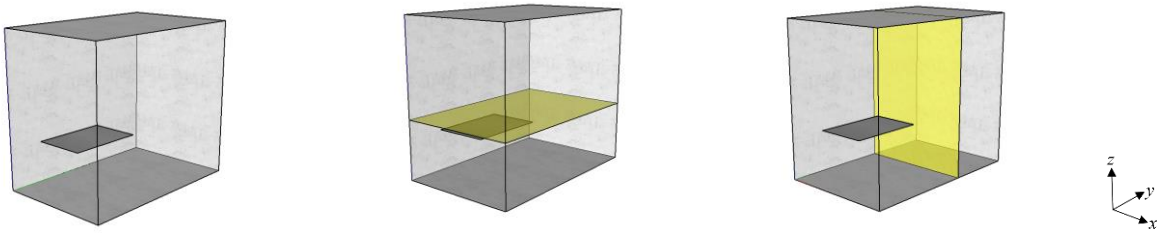

a) b) c)

Figure 1: Measurement grids inside the reverberant chamber

a) Empty room with plate b) Horizontal grid c) Vertical grid

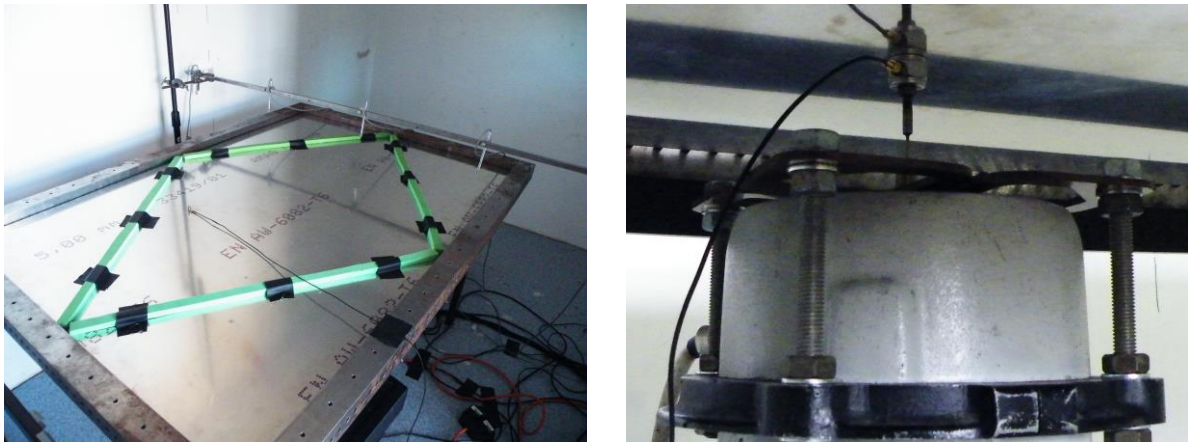

a) b)

Figure 2: Experimental set-up in the reverberant chamber

a) Plate with viscoelastic (green) material b) Electrodynamic shaker with force transducer

4. Results

Table 1 compares the first five plate eigenfrequencies from FDTD with measurements. Considering that the experimental set-up for the plate aimed to approximate simply supported boundaries, there is close agreement with FDTD (apart from a difference of 8% for the second mode).

Figure 3 allows comparison of measured and FDTD driving-point mobility (after accounting for the offset due to scaling with a factor s=6). Discrepancies in the frequencies at which the peaks occur (as noted in Table 1) but in general there is reasonable agreement.

Table 1: FDTD and measured eigenfrequencies

	Frequency (Hz)		
n	**Measured**	**FDTD**	**Difference (%)**
1	27.25	27.50	0.92
2	48.50	52.22	7.67
3	82.25	83.05	0.97
4	105.00	106.66	1.58
5	148.25	145.00	-2.24

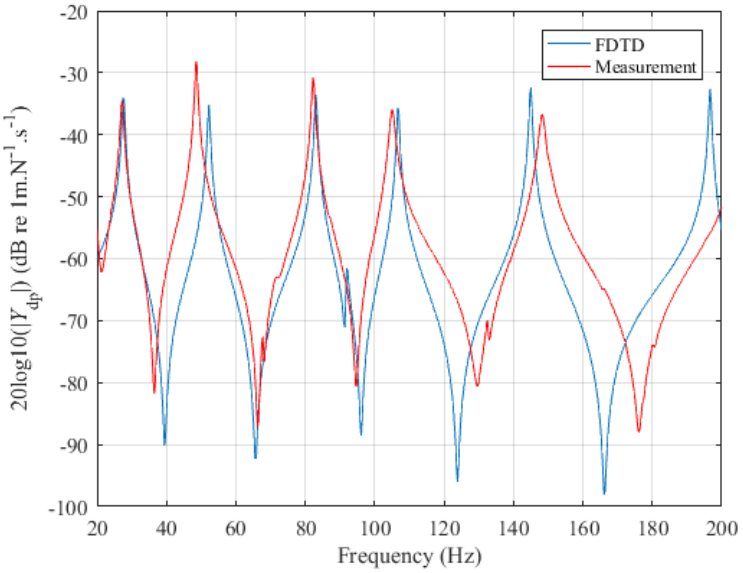

Figure 3: Measured and predicted driving point mobilities

The contour plots in Figs. 4 to 7 allow comparison of FDTD and measured pressure-to-force transfer functions (20lg|p/F|) for the horizontal and vertical measurement grids where the position of the plate is indicated using solid black lines. At ≈27Hz (Figs. 4 and 5) the fundamental vibration mode of the simply supported plate is visible and it is seen that although this is below the fundamental room mode (f_{100}=60Hz) there is close agreement between FDTD and measurements. The results for ≈92Hz are close to the f_{011} mode of the room (Figs. 6 and 7) and there is also close agreement between measurements and FDTD.

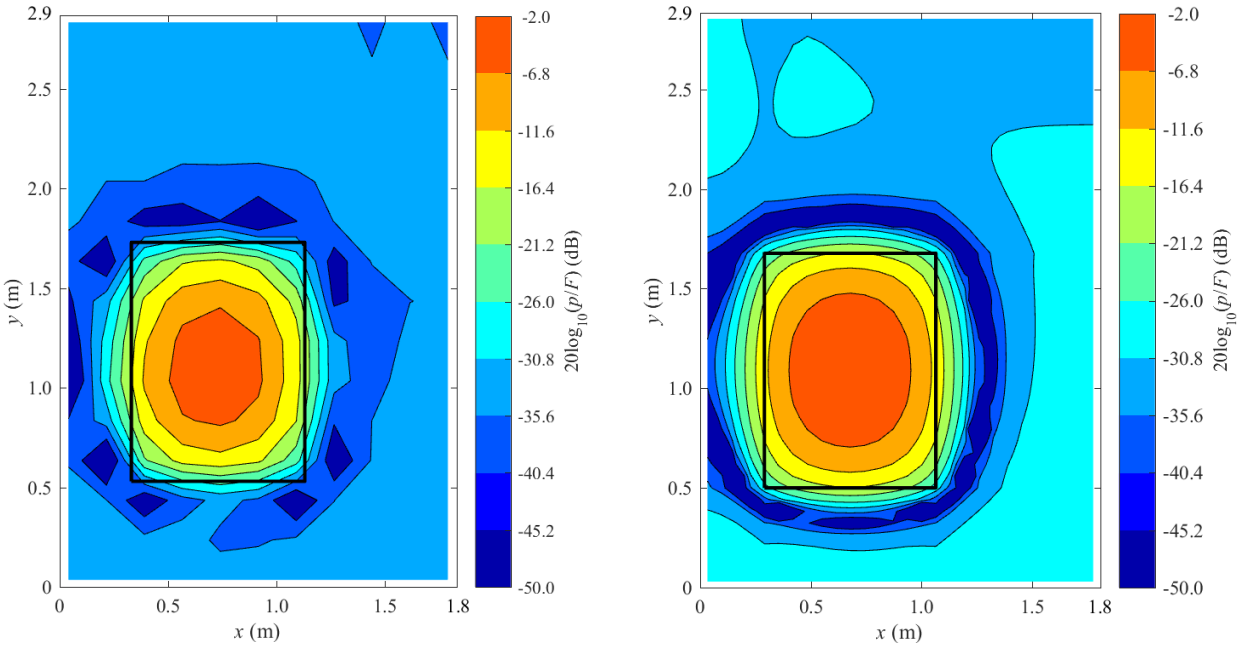

Figure 4: Measured (27 Hz, left) and FDTD (28Hz, right) transfer functions over the horizontal plane.

5. Conclusions

Experimental validation of an FDTD model has been carried out for the vibroacoustic problem of a thin plate undergoing point excitation inside a small reverberation chamber. For this model, the vibroacoustic scaling approach proposed in this paper significantly reduced the computation time.

Although not implemented here, it is possible for this scaling formulation to be parallelized to give further reductions in computation time.

The agreement between measured and FDTD eigenfrequencies of the plate confirms that the approach used to implement boundary conditions for the surface of the plate is correct. Close agreement between the measured sound field in the room and FDTD confirms that implementing a thin plate as a 3D solid that can support multiple wave types is valid.

Acknowledgement

The authors are very grateful to Dr Gary Seiffert (Acoustics Research Unit) for his help with all the measurements.

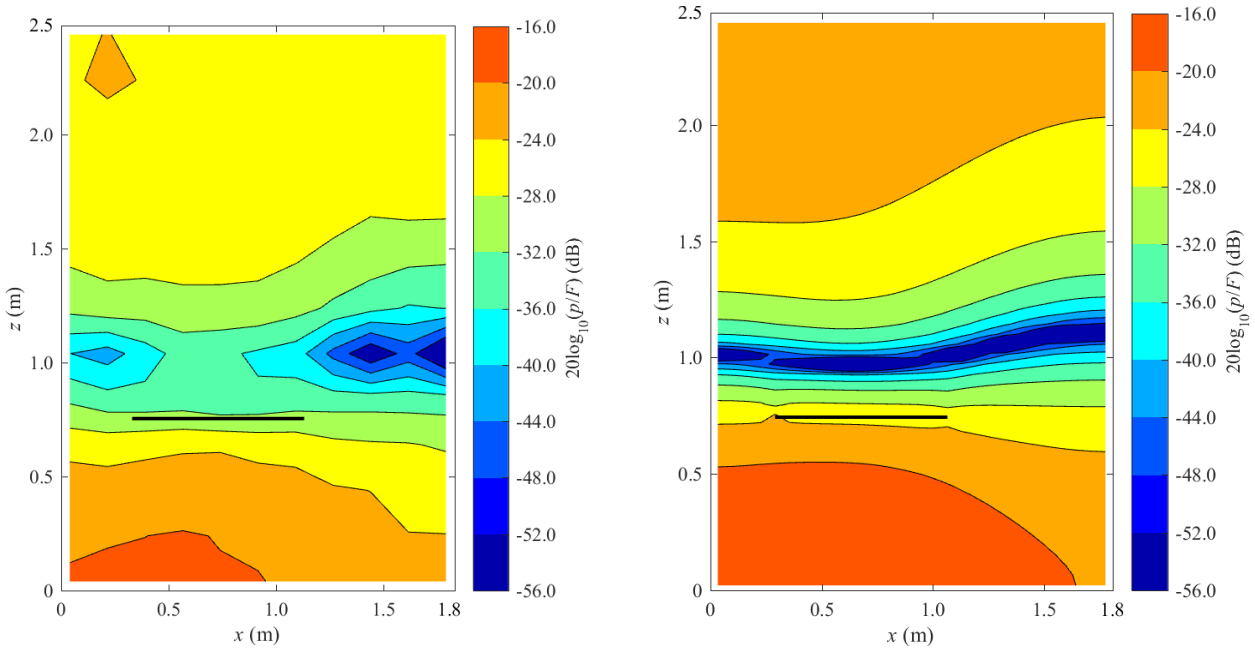

Figure 5: Measured (27 Hz, left) and FDTD (28Hz, right) transfer functions over the vertical plane.

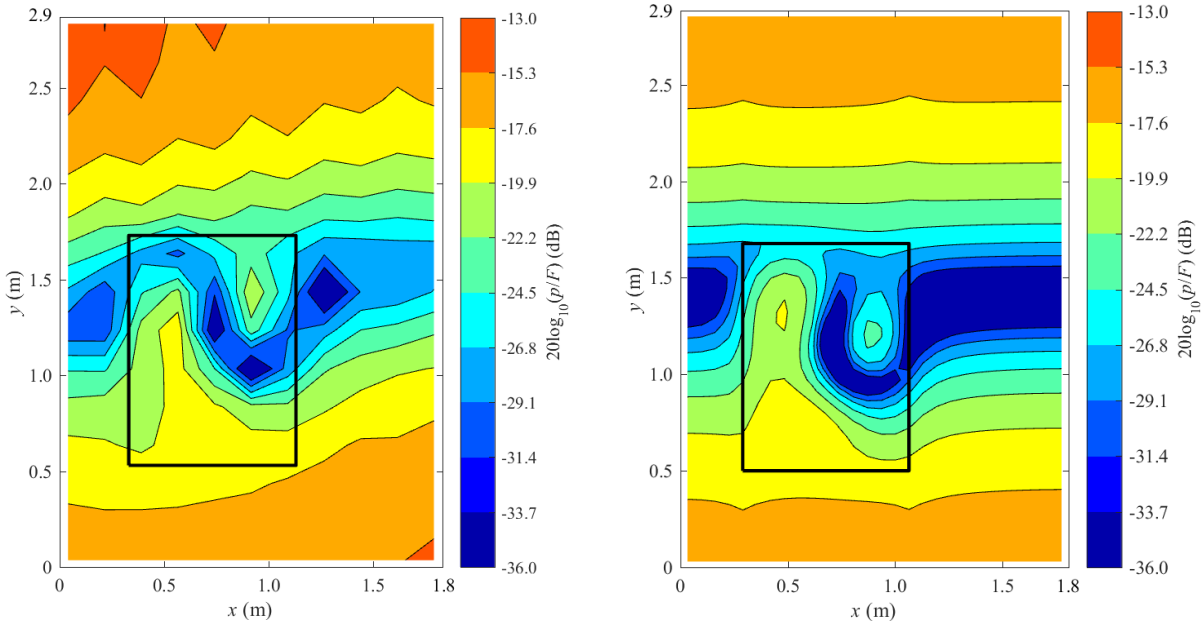

Figure 6: Measured (92 Hz, left) and predicted (90Hz, right) transfer functions over the horizontal plane.

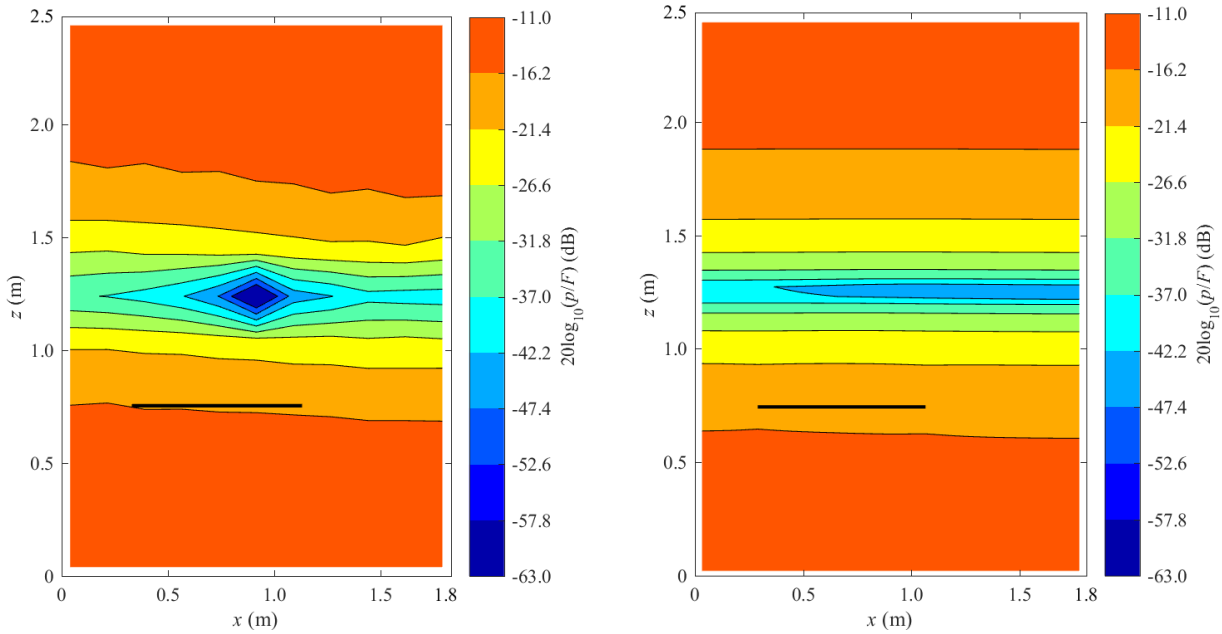

Figure 7: Measured (92 Hz, left) and predicted (90Hz, right) transfer functions over the vertical plane.

REFERENCES

1 Toyoda, M. and Takahashi, D., Prediction for architectural structure-borne sound by the finite-difference time-domain method, Acoustical Science and Technology, 30(4), 265-276, (2009).

2 Taflove, A., Hagness, S., Computational Electrodynamics, 3rd ed., Artech house, Boston, 2005.

3 Kurose, T., Tsuruta, K., Totsuji, C., Totsuji, H., FDTD simulations of acoustic waves in two-dimensional phononic crystals using parallel computer, Memoirs of the Faculty of Engineering, Okayama University, 43, 16-21, (2009).

4 Asakura, T., Sakamoto, S., Improvement of sound insulation of doors or windows by absorption treatment inside the peripheral gaps, Acoustical Science and Technology, 34(4), 241-252, (2013).

5 Asakura, T., Ishizuka, T., Miyajima, T., Finite-Difference Time-Domain analysis of structure-borne sound using a plate model based on the Kirchhoff-Love plate theory, Acoustical Science and Technology, 35(3), 127-138, (2014).

6 Asakura, T., Ishizuka, T., Miyajima, T., Prediction of low frequency structure-borne sound in concrete structures using the finite-difference time-domain method. Journal of the Acoustical Society of America, 136(3), 1085-1100, (2014).

7 Ferreira, N., Hopkins, C., Using finite-difference time-domain methods with a Rayleigh approach to model low-frequency sound fields in small spaces subdivided by porous materials, Acoustical Science and Technology, 34(5), 332-341, (2013).

8 Kunz, K. and Luebbers, R., *Finite Difference Time Domain Method for Electromagnetics*, CRC Press, Boca Raton (1993).

9 Bland, D., *The Theory of Linear Viscoelasticity*, Pergamon Press, New York (1960).

10 Schroder, C., Scott, W., Larson, G., Elastic waves interacting with buried land mines: a study using the FDTD method, IEEE Transactions on Geodesic and Remote Sensing, 40(6), (2002).

11 Yokota, T., Sakamoto, S., Tachibana, H., Visualization of sound propagation and scattering in rooms, Acoustical Science and Technology, 23(1), 40-46 (2002).

12 Yokota, M., Takahashi, D., Kawai, Y., Averaged material parameters and boundary conditions for the vibroacoustic finite-difference time-domain method with a nonuniform mesh, Acoustical Science and Technology, 33(4), 273-276 (2012).

13 Toyoda, M., Miyazaki, H., Shiba, Y., Finite-Difference Time-Domain method for heterogeneous orthotropic media with damping, Acoustical Science and Technology, 33(2), 77-85, (2012).

14 Hopkins, C., *Sound Insulation*, Elsevier, Amsterdam (2007). ISBN 978-0-7506-6526-1.

15 Yin, J. and Hopkins, C. Prediction of high-frequency vibration transmission across coupled, periodic ribbed plates by incorporating tunneling mechanisms. Journal of the Acoustical Society of America, 133(4), 2069-2081, (2013).